Radio Science

RESEARCH ARTICLE
10.1029/2018RS006607

Special Section:
URSI General Assembly and Scientific Symposium (2017)

Climatological Model of Over-the-Horizon Radar

M. A. Cervera[1,2], D. B. Francis[1], and G. J. Frazer[1]

[1]High Frequency Radar Branch, Defence Science and Technology Group, Edinburgh, South Australia, Australia, [2]School of Physical Sciences, The University of Adelaide, Adelaide, South Australia, Australia

Abstract Models of radar systems are required for a variety of reasons. The sophistication of these models is highly dependent on their purpose; for instance, microwave radar models, which are designed to be integrated into existing wargaming simulation frameworks, will often be low-fidelity models. The development of similar models of over-the-horizon (OTH) radar is particularly challenging. This is due to the highly variable propagation environment in which such systems are required to operate: even the lowest fidelity model of an OTH radar must model the environmental conditions appropriately. The *base level* environmental modeling required to accurately characterize OTH radar performance is the climatology, that is, diurnal, seasonal, and solar cycle variations. In this paper we detail a climatological model of OTH radar developed using high-frequency radio wave ray tracing techniques. We discuss how this model may be used to provide initial assessments of the viability of candidate OTH radar networks to meet particular missions and how it may be used in sophisticated radar network design methodologies.

Key Points:
- We develop a climatological model of over-the-horizon radar
- The model is demonstrated for the mission of surveilling commercial aircraft in the Australian eastern seaboard region
- The model may be used to design new systems or assess existing systems

Correspondence to:
M. A. Cervera,
manuel.cervera@dst.defence.gov.au

Citation:
Cervera, M. A., Francis, D. B., & Frazer, G. J. (2018). Climatological model of over-the-horizon radar. *Radio Science*, *53*, 988–1001. https://doi.org/10.1029/2018RS006607

Received 23 APR 2018
Accepted 26 JUN 2018
Accepted article online 6 JUL 2018
Published online 1 SEP 2018

1. Introduction

Sky wave over-the-horizon radar (OTHR) is a (high-frequency) HF radar technology that exploits the Earth's ionosphere to enable long range beyond horizon propagation of HF radar signals for the purpose of wide-area surveillance of aircraft and maritime vessels. The ionosphere is a highly variable medium, and this variability greatly influences the operational performance of a sky wave OTHR. Considerable care in selecting radar operating parameters is required to achieve optimal performance for the required mission and sophisticated modeling of OTH radar networks may be used to this end.

The performance of OTHR is governed by many factors. These are the propagation environment (the ionosphere), the physical radar equipment (transmitter power, transmit and receive antenna gains), the target scattering radar cross section (RCS), clutter from ground or sea backscatter which may be spread in Doppler due to ionospheric disturbances, the external noise environment of radar receiving system, radio frequency interference from other transmitters, the choice of radar waveform, the signal processing and target tracking algorithms, and the allocation of the radar resources (e.g., Skolnik, 2008).

In a companion paper (Francis et al., 2017), we discuss the development of a Radar Network Design Methodology, with reference to the above factors, and detail the associated metrics used to assess proposed OTH radar network designs. In this paper we focus upon the climatological model of the environment relevant to HF radio wave propagation which may be used to provide an initial assessment of the suitability of an OTH radar for a particular mission. Another application is the inclusion of low-fidelity but realistic models of OTH radar into existing wargame simulation frameworks.

2. Hypothetical Radar System Configuration

2.1. Overview

We develop and explore our OTH radar model using a hypothetical network of OTH radar. This hypothetical radar network is displayed in Figure 1 and is composed of three radars located in New Zealand, New Caledonia, and Norfolk Island directed toward the Australian eastern seaboard. The mission of this radar network is to monitor Boeing 777 commercial jet airliners in this region.

The translucent overlays in Figure 1 are the notional coverage regions of each radar and is typical of OTH radar. The azimuth extent is 90°, and the range extent from 1,000 to 3,000 km. The actual coverage area is dependant on the ionospheric conditions and may well be less than displayed during winter, solar minimum, or predawn when the propagation conditions are poor. The white lines indicate commercial flight paths between

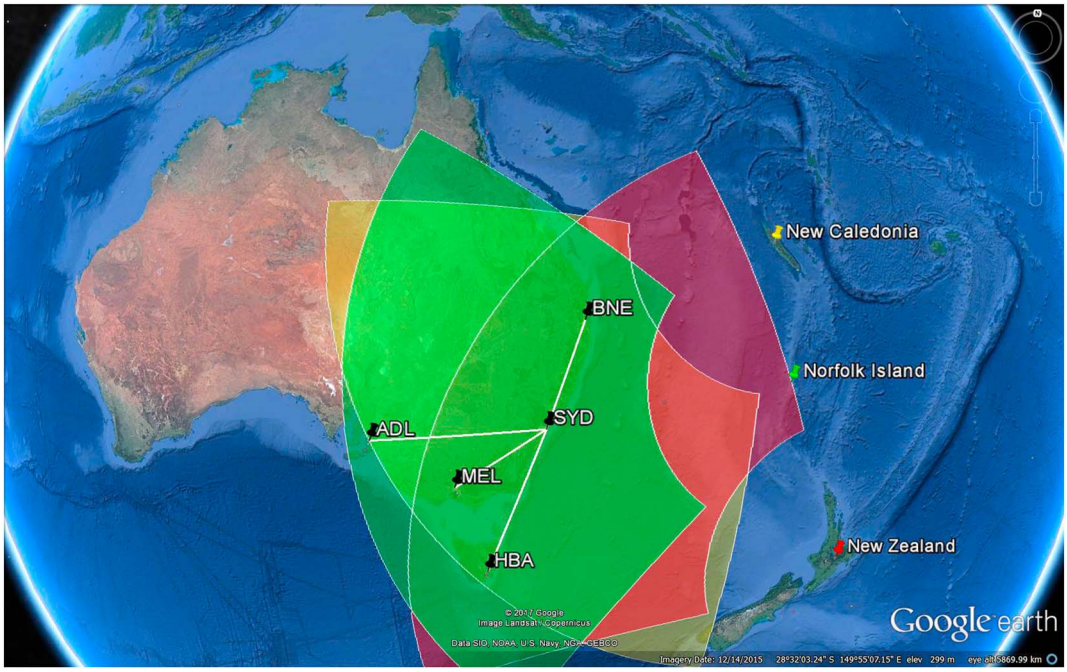

Figure 1. Hypothetical radar network with over-the-horizon radars located at New Zealand, New Caledonia, and Norfolk Island directed to monitor the Australian eastern seaboard.

the major Australian cities and Sydney. The model will be used to predict radar performance of tracking commercial airliners flying along these routes.

Each OTH radar system is identical and has the characteristics described in the following subsections. The antenna arrays are modelled by using the Numerical Electromagnetics Code (NEC)-4 (Burke et al., 1979). The locations and boresites of the radars is given in Table 1.

2.2. Transmit System

The transmit array is modeled as a linear array of 16 log-periodic dipole antenna (LPDA) elements (e.g., Krauss, 1998) designed to operate in the 13- to 26-MHz band. We note that OTH radar typically are able to operate down to 5-MHz. The frequency limitation of our model system is a deliberate choice to explore the performance of a scaled down system, which will have a lower design cost. In order to operate in the 5- to 13-MHz frequency band, a second *low-band* transmit array would be required to be constructed at considerable additional cost due to the larger size of these array elements.

The interelement spacing of the array is 6 m. Each LPDA element is composed of 17 dipoles with a spacing factor (ratio of dipole spacing to 4 times dipole length) sigma of 0.1. This requires an antenna mast of ~ 24 m with a curtain length of 26.4 m. The dipole and feedline wire diameters are 7 mm, and the input impedance of each LPDA is 300 Ohm. A 20-dB Taylor amplitude taper (nbar = 2) was applied across the array for sidelobe control. The LPDA are fed by individual 5-kW (peak) power amplifiers for a total of 80 kW (peak) supplied to the array. A pattern enhancing ground screen of 250- ×250-mm mesh extending 200 m in front of the array and 10 m behind was included in the model.

Table 1
Radar Locations and Boresights of the Hypothetical OTH Radar Network

	Radar site		
	New Zealand	New Caledonia	Norfolk Island
Latitude	−38.853°	−21.095°	−29.016°
Longitude	176.425°	164.948°	167.940°
Boresight	276.0°	221.0°	247.0°

Note. OTH = over-the-horizon.

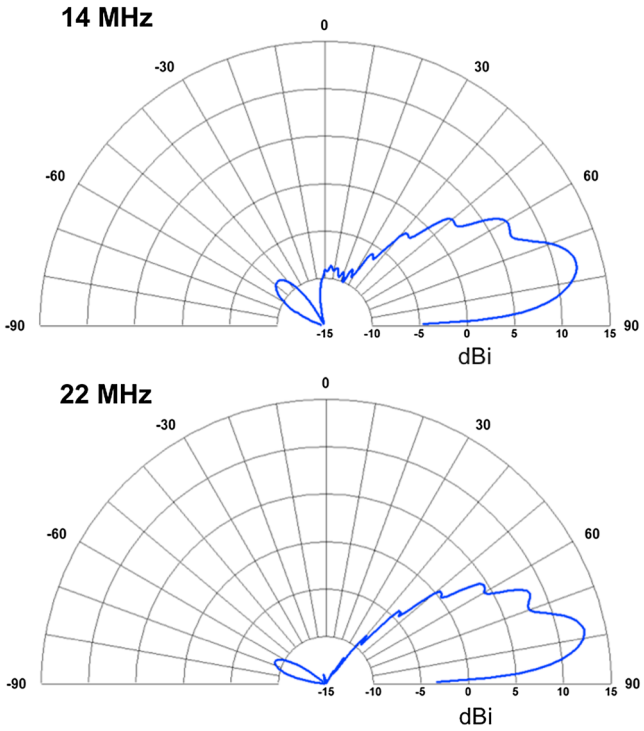

Figure 2. Elevation pattern at 0° azimuth of a single log-periodic dipole antenna element at 14 MHz (top) and 22 MHz (bottom).

Antenna array gains were generated at 0.5-MHz frequency steps using NEC-4 at a resolution of 0.5° in elevation and 1.0° in azimuth for beam steer angles of −45–45°. Figure 2 displays the elevation pattern of a single LPDA at an azimuth of 0° at two frequencies, while Figure 3 displays the directive gain of the entire array (i.e., the maximum gain of the beam when the array is phased such that a beam is formed in a particular direction) at the same two frequencies. Note that the surface of constant phase for a linear array has the shape of a cone. Thus, the steer azimuth, ϕ_{steer}, of the array required to illuminate a target at a given ground azimuth, ϕ_{target}, will vary as a function of the ray elevation, β. The relationship is given by $\sin(\phi_{\text{steer}}) = \sin(\phi_{\text{target}})\cos(\beta)$.

2.3. Receive System

A typical OTH radar receive array arrangement is a linear array of doublet antennas. We assume in our model that the OTH radar system will be externally noise limited (i.e., the external environmental noise received by the system is much greater than the internal noise of the receivers) noting that this may not be able to be achieved under all propagation conditions. This simplifies the design of the receive antenna elements considerably as they are not required to be frequency broadbanded as for the transmit antenna elements.

In this paper we model the receive array of our hypothetical system as a linear array of 64 doublet monopole elements (Lomasney & Sweeney Jr, 1973) with an interelement spacing of 6.4 m. A pattern enhancing ground screen of 250- × 250-mm mesh extending 50 m in front of the front monopole and 7.5 m behind the rear monopole was included in the model. The monopoles have a height of 5.0 m with a front to rear monopole spacing of 3.7 m. The rear monopole is phase shifted by π radians and when the two are combined forward directivity is gained in the antenna pattern with a null in the reverse direction. A 30-dB Taylor (nbar = 4) amplitude taper was applied across the array for sidelobe control. We note that modern OTH radars employ a digital receiver per element with the amplitude taper applied at the digital beamforming stage. When applying the amplitude taper to our array, the weights of the amplitude taper were normalized in a manner to ensure the noise power would also be normalised. Thus, we can assume the modelled reduction in directive gain is indicative of the losses incurred by the digital beam former.

The antenna array gains were generated using NEC-4 at the same frequency, elevation and azimuth resolution as for the transmit array. Figure 4 displays the elevation pattern of a single doublet at an azimuth of 0° at two

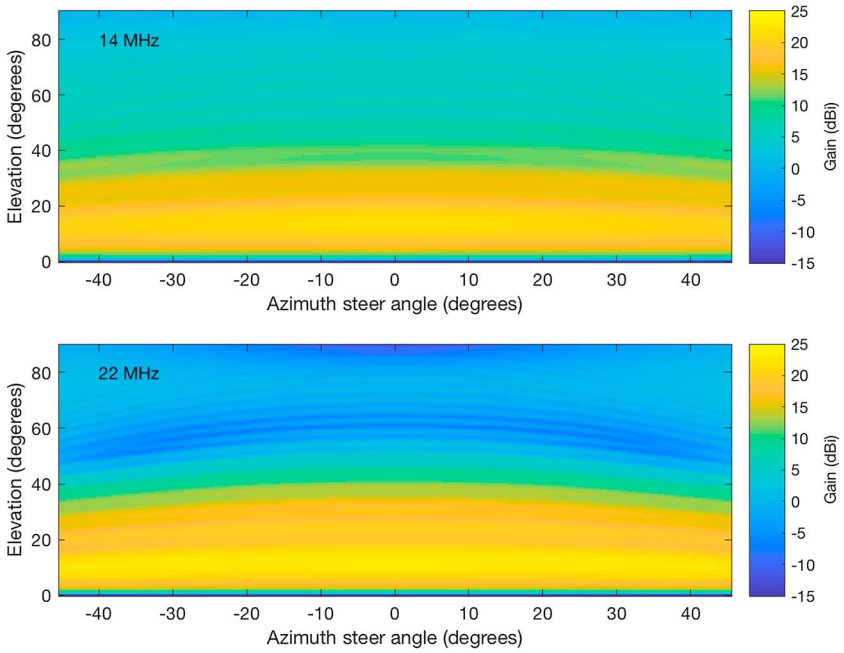

Figure 3. Directive gain of the log-periodic dipole antenna transmit array at 14 MHz (top) and 22 MHz (bottom).

frequencies, while Figure 5 displays the directive gain of the entire array. The same remarks as for the transmit array regarding steer azimuth versus target azimuth apply.

3. HF Propagation Model

Core to the operation of OTH radar systems is the propagation of HF radio waves beyond the Earth's horizon via the ionosphere. We employ numerical radio wave ray tracing techniques to model the propagation of the HF

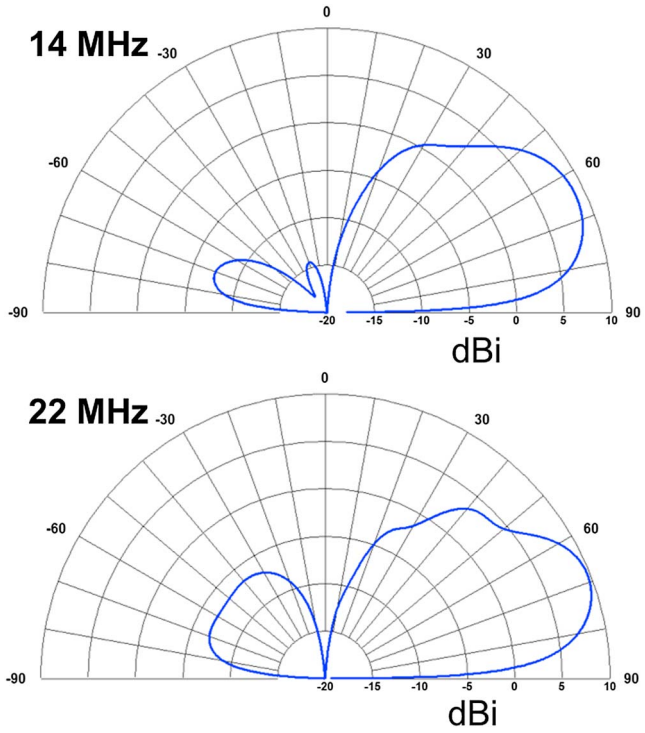

Figure 4. Elevation pattern at 0° azimuth of a single doublet element at 14 MHz (top) and 22 MHz (bottom).

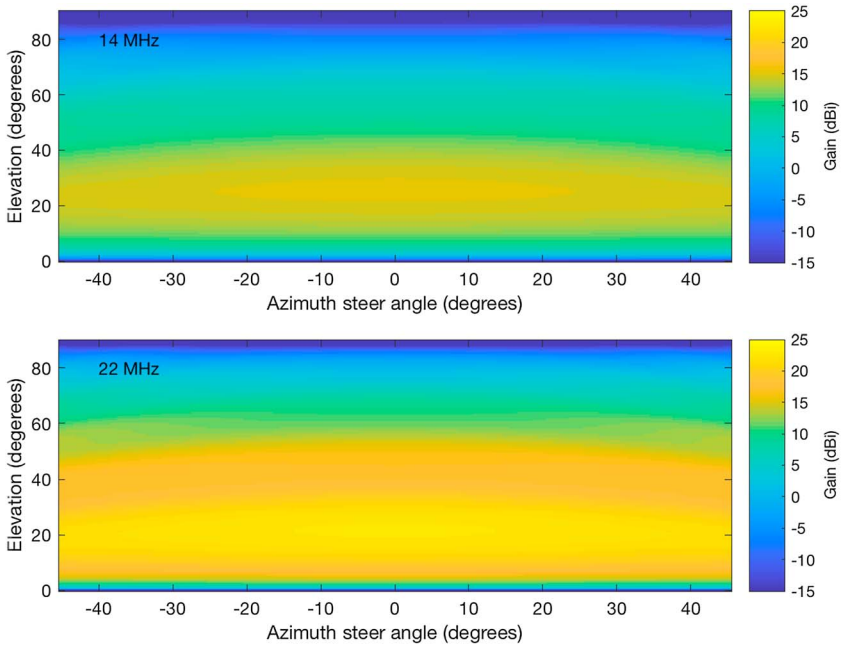

Figure 5. Directive gain of the 64 doublet element receive array at 14 MHz (top) and 22 MHz (bottom).

signals through a monthly median model of the ionosphere viz., the 2016 International Reference Ionosphere (Bilitza et al., 2014). In our work we use the PHaRLAP (Cervera & Harris, 2014) ray tracing toolbox developed by one of the authors. Figure 6 displays an example of one-way raypaths calculated using PHaRLAP's 2-D numerical ray tracing (NRT) engine, which is based on the algorithms developed by Coleman (1998). It is possible to use 3-D NRT, which includes the effects of out-of-plane ionospheric tilts and the geomagnetic field. However, this comes with a large speed-of-computation penalty, and for our purposes 2-D NRT is sufficient.

Lucas et al. (1993) have previously developed HF propagation modeling tools for the purpose of assessing OTH radar systems. While their propagation model was suitable for their purposes at the time, we note that it

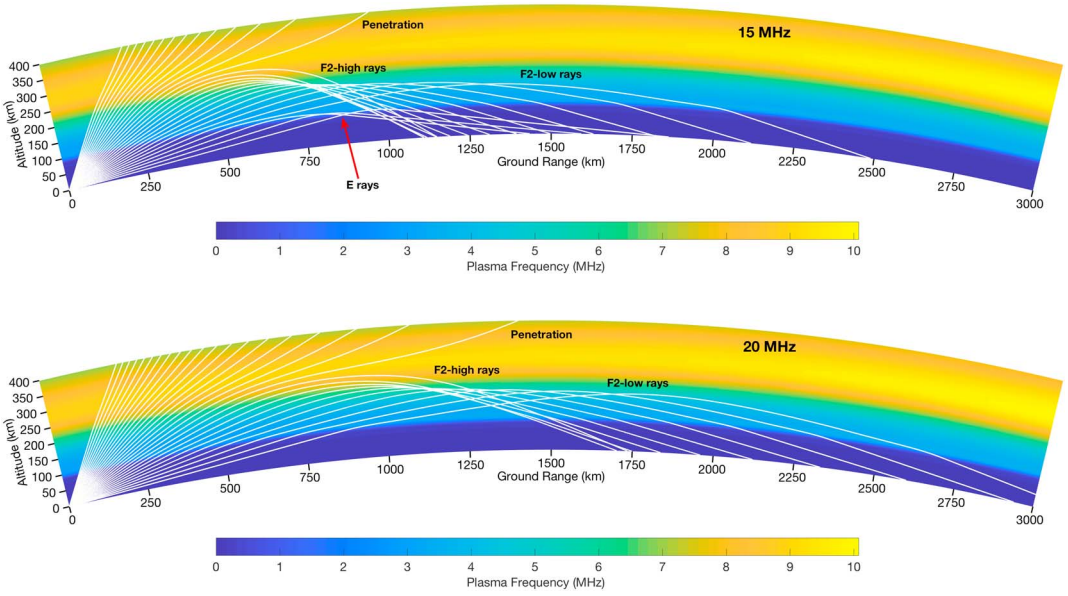

Figure 6. Example of one-way raypaths for (top) 15 MHz and (bottom) 20 MHz rays calculated by 2-D numerical ray tracing for a radar located in New Zealand during daytime, summer, solar maximum conditions directed toward Sydney, Australia (*az*. = 276°). Note the different ionospheric propagation modes, the ionospheric penetration by the high elevation angle rays, and the larger skip distance for higher-frequency rays.

is less sophisticated than our model detailed here. Their model assumes a spherically symmetric ionosphere where the downrange gradients are negligible. Model vertically incident ionograms are calculated from which oblique paths are obtained using equivalent geometry techniques. We note that this model would not be suitable for assessing OTH systems operating near the equatorial regions where the downrange ionospheric gradients are large. Furthermore, they do not consider aspect sensitive RCSs of the targets of interest, target tracking algorithms, or the allocation of radar resources which we do in later sections.

It is beyond the scope of this paper to discuss in detail the effect of the morphology of the ionosphere on the raypaths; however, we note that there is often more than one propagation mode to a particular ground range. In this example we see E, F2-low (F2L), and F2-high (F2H) propagation modes. In general, for a quasi-monostatic system ($\sim$ 80-km transmit-receive site separations are usual for OTHR to meet site isolation requirements), if there are N propagation modes to a target then there are a total of N^2 modes that are available to return energy to the receiver. In the example displayed in the top panel of Figure 6 energy propagates out to a ground range of 1,400 km via an E mode and an F2L mode. Thus, targets at this range will return four echoes corresponding to the following outbound-inbound modes: E-E, E-F2L, F2L-E, and F2L-F2L. Each of these modes will typically have a different group (or radar) range, elevation angle at the receive array, and power. The two *crossed* modes will appear at the same group range, and so one may expect three echoes to be observed by the radar receive system for a single target (in this example). OTH radar systems will typically try to detect and form tracks on each of these modes.

Closer to the skip zone there are no E layer propagation modes; however, there exists two propagation modes via the F layer, viz., the F2-low mentioned previously and an F2-high mode. The same comment regarding outbound and inbound mode combinations apply except they are now F2L-F2L, F2L-F2H, F2H-F2L, and F2H-F2H. Under certain circumstances propagation modes also exist via the F1 layer (all F modes depicted in this example are F2 layer propagation modes) and so one can appreciate that the mode structure of target echoes can become complicated for OTH radar.

The bottom panel of Figure 6 shows that radio waves at a higher frequency (20 MHz in this case) propagate out to longer ground ranges. Careful selection of the radar operating frequency is required for the ground range of interest to be surveilled. In the example shown in Figure 6 a target at 1,500 km would not be observed by the radar operating at 20 MHz as the target is inside the skip zone; however, a frequency of 15 MHz is suitable. Conversely, while a target at 2,000 km is illuminated by radio waves at 15 MHz, defocusing effects are large. In this case a frequency of 20 MHz is more suitable.

In order to characterize the signal propagation properties of each radar in the network, we calculate propagation lookup tables over a range of environmental conditions: this includes the equinoxes and solstices at low-, middle-, and high-solar activity levels. We use the 12-month smoothed Zurich sunspot number (SSN) as measure of the solar activity (Davies, 1990). Note that 2016 International Reference Ionosphere still requires the V1.0 sunspot number to be input and all SSN values quoted herein are V1.0. Ionospheric propagation effects such as ray focusing (Davies, 1990) and radio wave absorption are included. The ionospheric absorption model used is that due to George and Bradley (1974). We make the simplifying assumption that the transmit and receive systems are colocated.

Ray homing techniques (Coleman, 1997) are used with the 2-D NRT results to calculate, for a given radar operating frequency, the various quantities of interest at the target ground range: group range, ray elevation, absorption loss, and focusing gain/loss. This allows us to calculate the predicted received signal power as a function of target range and frequency via the standard radar equation with additional terms included for the absorption and focusing effects:

$$P_R = \frac{\lambda^2 \sigma P_T G_T G_R}{(4\pi)^3 L_T L_R R_{e,T}^2 R_{e,R}^2} \tag{1}$$

where λ is the wavelength, σ the target RCS, P_T the transmitted power, G_T and G_R the transmit and receive gains, L_T is the ionospheric absorption for the outbound (i.e., transmitter to target) path, L_R is the ionospheric absorption for the inbound (i.e., target to receiver) path, and $R_{e,T}$ and $R_{e,R}$ are the outbound and inbound effective ranges. The effective range is calculated from the actual distance traveled by the ray and the change in cross-sectional area of the flux tube represented by the ray. Thus, the effective range takes into account focusing gains or losses (Coleman, 1997; Davies, 1990).

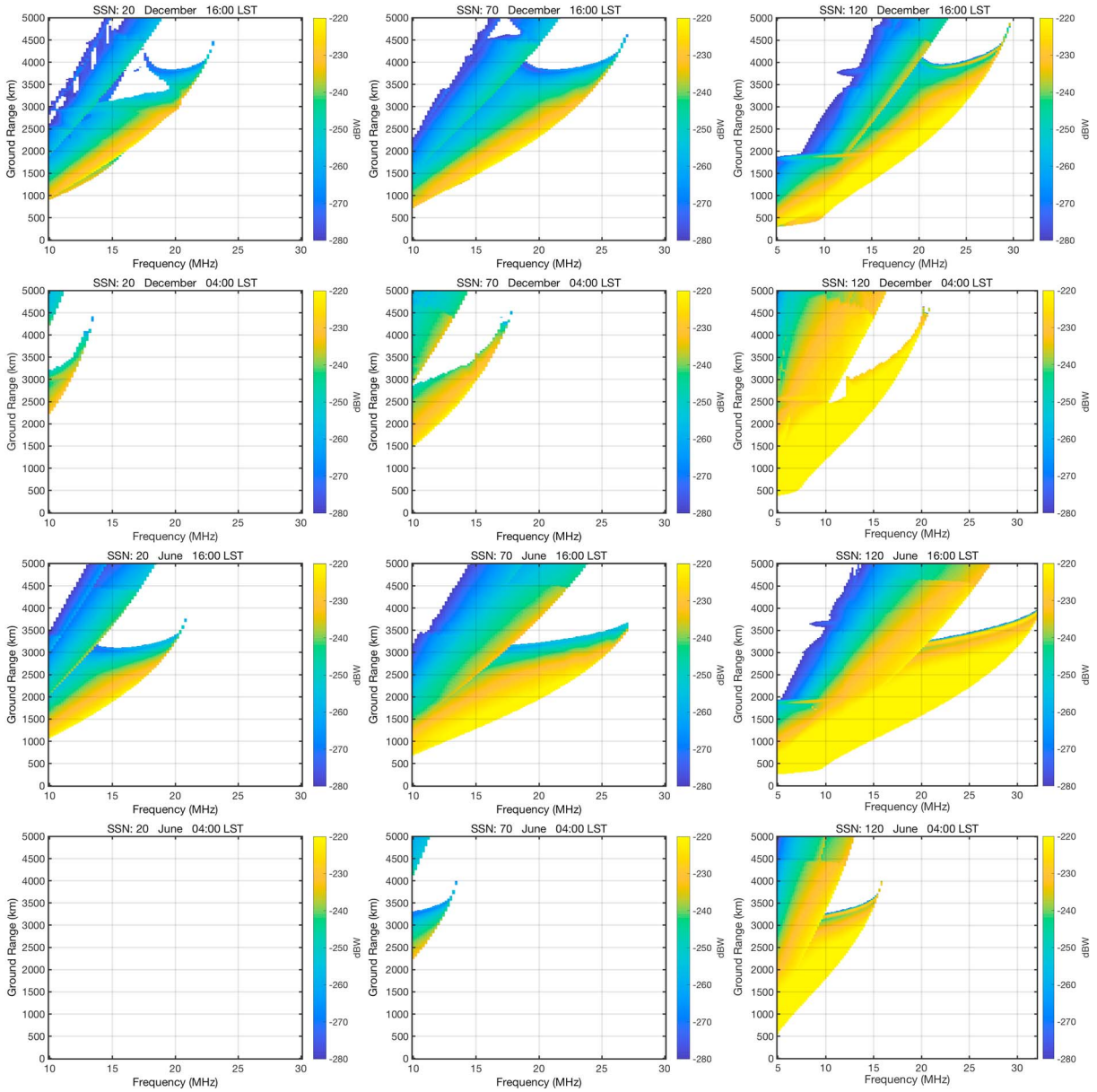

Figure 7. Example of the varying propagation conditions for the New Zealand hypothetical radar. (left column) Low solar activity, (middle column) middle solar activity, and (right column) high solar activity. (first row) daytime summer, (second row) night summer, (third row) day winter, and (fourth row) night winter. The radar cross section is 1 m^2 and the transmitter power 1 W. The time standard for these plots is local solar time (LST) at the radar. SSN = smoothed sunspot number.

The tables take the form of predicted received power from a 1-watt (W) radiator assuming a 1-second (1-s) coherent integration time (CIT), and a target with 1-m^2 RCS. The tables are parameterized by radar-to-target ground range and radar operating frequency, with transmit and receive antenna patterns and array gains included. As noted previously, there may be several propagation modes to a particular ground range; only the strongest mode is retained for the construction of the tables. The range resolution of the tables is 15 km, and the frequency resolution 0.2 MHz. The elevation information of the ray at the target location is also stored. This is important when scaling the model power data from the tables with the target RCS due to its aspect sensitivity. The tables are constructed for each look direction of interest which in our case is the full 90° coverage arc of each radar at 2° resolution.

Figure 7 displays, graphically, propagation tables for the hypothetical radar located in New Zealand directed at Sydney, Australia, over a range of ionospheric conditions. These figures show that the ionospheric conditions have a great impact upon the OTH radar propagation support. Indeed, predawn (when the ionosphere is

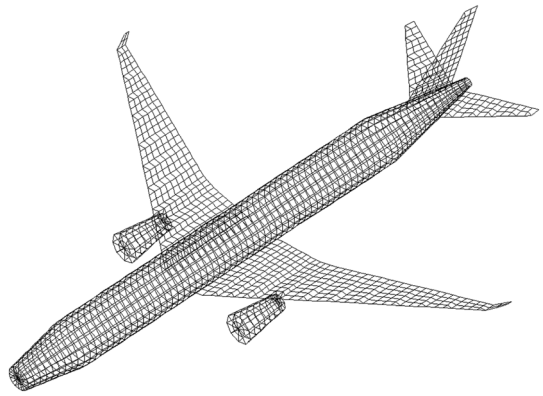

Figure 8. Wire frame model of a Boeing 777 aircraft used with Numerical Electromagnetics Code-4 to generate the radar cross section of the targets of interest (commercial jet aircraft).

weakest) during winter at solar minimum there is no propagation support at all for frequencies above 10 MHz. Propagation modelling (not shown here) indicates that an OTH radar at this location would have to operate at frequencies near 5 MHz during these conditions. This would require a dual-band transmit array design which would increase the complexity and cost of any such system.

4. Target RCS

The class of targets monitored by OTH radar have physical sizes which are, to first order, similar to the wavelength of the radar signals. Consequently, the target RCS may vary greatly with the frequency and the angle of incidence of the illuminating radio waves. Thus, we need a realistic model to the target RCS, which captures this variability. Computer wire frame models of our targets of interest were used with NEC-4 to model the frequency and aspect dependant RCS. The targets are Boeing 777 jet airliners, which are typical of the commercial aircraft flying along the Australian eastern seaboard. The RCS model data were generated at a frequency resolution of 0.5 MHz and elevation and azimuth resolutions of 1°.

Figure 8 displays the wire frame model used to model the Boeing 777 aircraft and Figure 9 the aspect sensitive RCS data generated by NEC-4 at two frequencies for the vertical and horizontal polarization cases. A cursory inspection of these figures shows that the RCS is highly dependent on the aspect of the target, the frequency of the incident radio waves and the polarization.

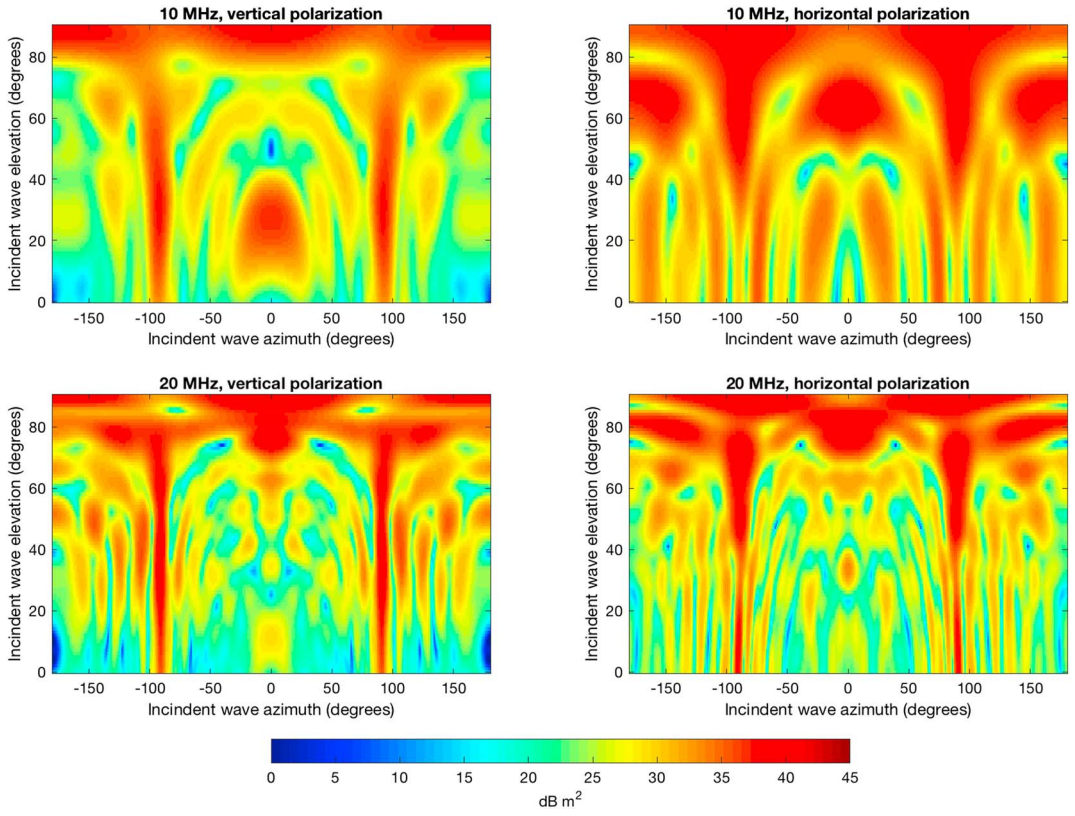

Figure 9. Model radar cross section of a Boeing 777 calculated by Numerical Electromagnetics Code using the the wire frame model displayed in Figure 8. The incident radiation is (top) 10 MHz and (bottom) 20 MHz and the polarization (left) vertical linear and (right) horizontal linear. The aspect angles are referenced such that elevation and azimuth of 0° is in the direction along the aircraft fuselage toward the tail.

In general, while the polarization of the transmitted radio waves is known (typically linear vertical), the polarization is unknown when the radio waves exit the ionosphere. The radio waves split into the two canonical propagation modes viz., the ordinary (O) and extraordinary (X) polarization modes due to the anisotropy of the ionospheric refractive index and will in general be elliptically polarized with their polarization vectors rotating in the opposite sense. However, the eccentricity of the polarization ellipses and the orientation of the major axes are unknown. It would be possible to calculate the polarizations using 3-D NRT and knowledge of the geomagnetic field, but that is beyond the scope of this paper, and indeed, that level of model fidelity is unnecessary for the purpose of the OTH radar model described herein.

To proceed, we require an adequate approximation for the RCS of the target based on our NEC modeling of the linear vertical and horizontal cases. We note that these cases may be regarded as limiting cases of the general elliptically polarized radio waves. As the target moves along its trajectory the orientation of the polarization ellipse of the illuminating radio waves with respect to the target will change. For our purposes we wish to characterize the average response from the target, not the peak nor the worst performance. Thus, for the purpose of our model results presented in this paper we assume that the RCS can be characterized, to first order, as the maximum value of these two linear cases less 3 dB.

5. Model Application

5.1. Initial Assessment and Sensitivity Analysis

Anticipated target signal-to-noise ratio (SNR) is calculated from the aforementioned propagation tables by scaling the power by the radar parameters (transmit power and CIT), using a proposed target RCS and an appropriate background noise model. The internal noise of the receivers is not considered as well-designed OTH radar are externally noise limited. For a target ground range of interest the propagation frequency which maximises the SNR is chosen. This frequency is typically close to the *leading edge* where skip focusing occurs (Davies, 1990). We apply an additional restriction; the choice of frequency is not allowed to exceed the value 1 MHz back from the leading edge. This is to simulate how OTHR are operated; frequencies too close to the leading edge leave the radar susceptible to losing propagation support if the ionospheric conditions change rapidly (e.g., at times around the dusk terminator or due to ionospheric disturbances).

For the noise estimate we used a simple rural International Telecommunication Union (ITU) median model for the background noise at the New Zealand radar site (International Telecommunication Union, 2013) and residential ITU at New Caledonia and Norfolk Island. The higher man-made noise level was chosen for the latter two sites to reflect the fact that the lack of space on those small islands mean it would be unlikely that a radio quiet site would be available. While the ITU models were sufficient for our purposes, more sophisticated directional models can be used if desired (Pederick & Cervera, 2016).

Various signal processing losses must be accounted and are typically 10 dB (Skolnik, 2008). These losses are due to (1) tapering applied during digital beamforming and range-Doppler processing to reduce azimuth, range, and Doppler sidelobe levels ($\sim$ 7 dB), (2) straddling or scalloping losses ($\sim$ 1.5 dB), and (3) ground clutter suppression (*whitening*) losses ($\sim$ 1.5 dB). Note that we do not include the digital beamforming taper losses in what follows as they have already been included in the model of the antenna pattern of the receive array (see section 2.3).

We combine all the parameters so far into an estimate of SNR of the target in the detection stage of the radar system:

$$\mathrm{SNR} = \frac{G_p P_{tx} T_{\mathrm{cit}} \sigma}{L_{\mathrm{sig}} N}, \tag{2}$$

where G_p is the base system propagation path losses and array gains generated by ray tracing as described previously, T_{cit} is the CIT gain relative to 1 s, P_{tx} is the transmitter power gain relative to 1 W, σ is the target RCS relative to 1 m^2, L_{sig} is the signal processing losses, and N is the noise power spectral density in decibel Watt per Hertz.

Radar target detection and tracking algorithms may now be applied. However, to gain an initial assessment of the suitability of an OTH radar system for a particular mission a simple tracker threshold may be used. If the target SNR exceeds the notional tracker threshold then the target may be considered to be successfully detected and tracked. By way of example Fabrizio (2013) suggests a tracker threshold of 15 dB and if the SNR exceeds this value we may consider the target to be successfully tracked.

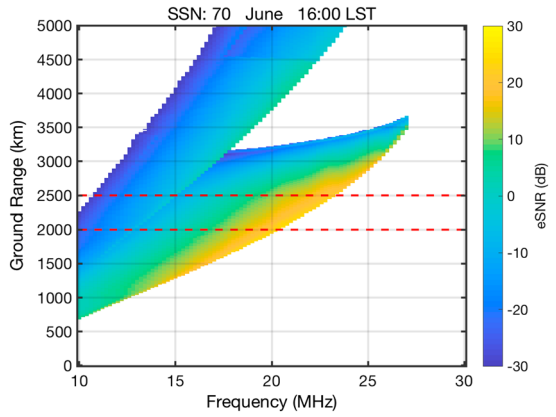

Figure 10. Example of excess signal-to-noise ratio; red dashed lines indicate region of surveillance interest.

Figure 10 displays excess SNR (eSNR), the level by which the target SNR exceeds the tracker threshold, for the hypothetical New Zealand radar directed toward Sydney (*az*. = 276°) at 16:00 LST during June and SSN = 70. The receive system CIT is 4 s, and the target a commercial jet airliner flying radially inbound to the radar (RCS ~ 30 dB m^2). If we are interested in tracking targets in the 2,000–2,500 km range window (indicated by the red dashed lines) then a choice of operating frequency of ~ 20 MHz is appropriate. The eSNR varies from 25 dB (at 2000 km) down to 11 dB (at 2500 km). A longer CIT will increase the eSNR of the target (noting that ionospheric variability limits the CIT to be typically no more than 60 s due to loss of signal coherence) but that comes at the expense of radar resource allocation which we discuss in the next section.

Target dynamics must be considered and consequently so too ground clutter. For the level of fidelity required for an initial assessment of our hypothetical radar network a simple ground clutter model with uniform backscatter coefficient (Earth RCS per unit area) is deemed sufficient. The clutter is assumed to be confined to a Doppler band corresponding to no more than ±46.3 km/hr. (i.e., the ionosphere is undisturbed and so the clutter is not spread in Doppler beyond this equivalent velocity). If the target radial speed is less than 46.3 km/hr, then we assume it has been obscured by the ground clutter and will not be detected.

We justify the use of this simple model of ground clutter based upon the relatively benign ionospheric conditions expected to be present in the midlatitudes that our hypothetical OTH radar system would operate. However, OTH radar operating in equatorial regions, where the ionosphere may be disturbed and ionospheric irregularities may be present at certain times, will potentially experience Doppler broadening of the ground clutter. OTH radar operating in these regions must consider the effects of spread Doppler clutter during these times.

We note that an OTH radar model that is to be integrated into a wargaming simulation framework might also employ the simple clutter model detailed above. In this case the fidelity of the OTH radar model is governed by the overall fidelity of the wargaming framework.

While this simple model of ground clutter is appropriate for assessing the utility of OTH radar for tracking fast moving aircraft, we recognize that is not the case for slow-moving surface targets (e.g., ships). Slow moving targets will, no matter their direction of motion with respect to the radar, have radial speeds close to the ground clutter. For these targets it is extremely important to accurately characterize the ground clutter. Sophisticated HF channel simulation methods such as HiCIRF (Nickisch et al., 2012) are required for this class of target.

From the type of data in Figure 10 we are able to construct sensitivity maps of radar performance for a given time, month, and solar activity level of interest by calculating optimal frequency and SNR (or eSNR) at each ground range cell. This is repeated for each azimuth, and the result for the New Zealand radar at 16:00 LST during June and SSN = 70 for Boeing 777 aircraft flying inbound to Sydney at a typical cruising speed of 900 km/hr is displayed in Figure 11. As the propagation lookup tables also include the elevation of the radio waves incident on the target we are able to construct the same type of display of elevation. As expected, the elevation decreases as range increases.The two arcs where there are no data in the SNR plot is due to the target flying tangentially to the radar and is obscured by the ground clutter. The curved striations are due to the aspect sensitivity of the target RCS.

For the purpose of an initial assessment of the suitability of the radar to meet the mission requirements, an examination of the SNR over the coverage region with reference to a notional tracker threshold is essential. For the notional tracker threshold suggested by Fabrizio (2013) we require the SNR to exceed 15 dB. Under this requirement Figure 11 suggests that while tracking a Boeing 777 with this class of radar is feasible for the aircraft flying the Brisbane-Sydney and Melbourne-Sydney routes, the Hobart-Sydney flight path is marginal for the propagation conditions.

This style of analysis should only be the initial step in evaluating or designing an OTH radar system. While these plots are useful in indicating how a given radar may perform for the given environmental conditions they must ultimately be treated with caution. Target detection and tracking algorithms have not been modeled,

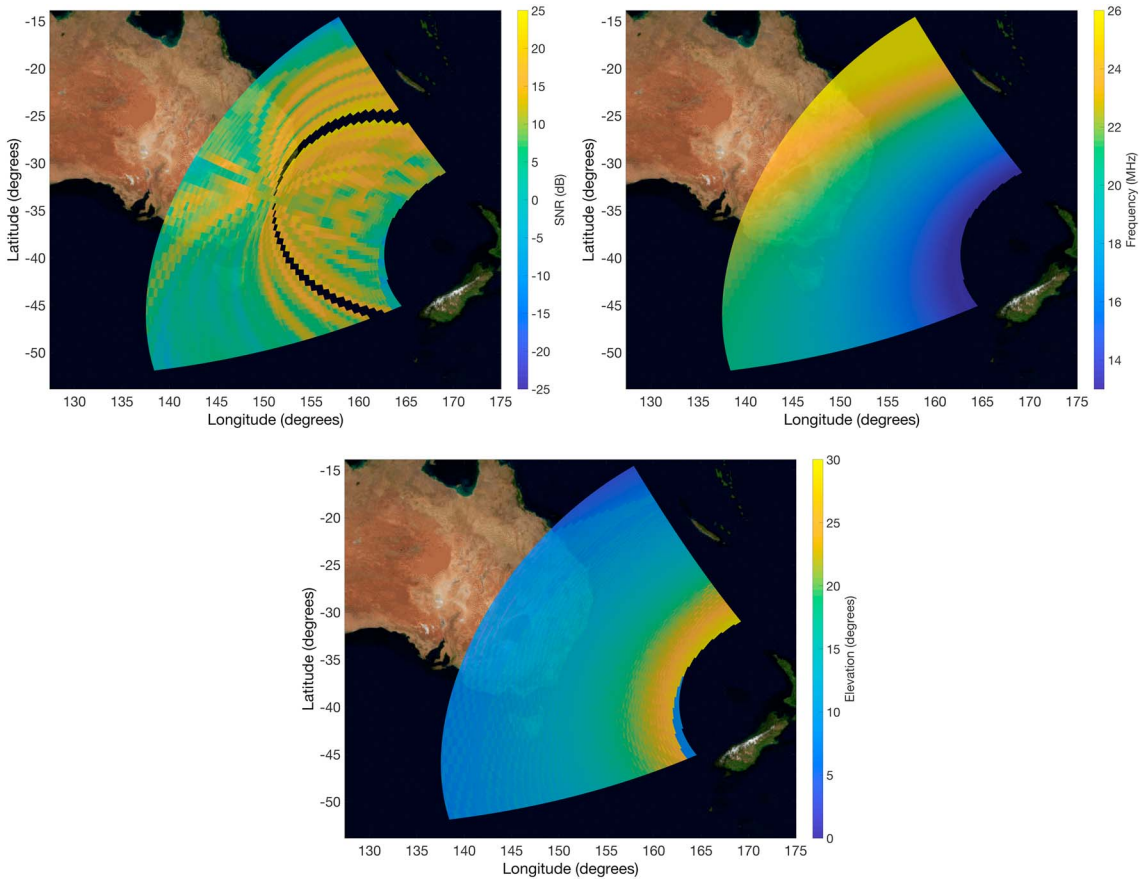

Figure 11. Example of (top left) optimal signal-to-noise ratio, (top right) optimal frequency, and (bottom) ray elevation at 16:00 LST during December and SSN = 70 for a Boeing 777 flying inbound to Sydney at each range-azimuth cell in the coverage area of the New Zealand radar. The aircraft is assumed to be nonmanoeuvring (i.e., always radially inbound to Sydney) at a typical cruising speed of 900 km/hr.

and the decrease in SNR with range over a surveilled region is not included (i.e., in practice one cannot choose the optimal operating frequency for every ground range cell), and radar resource allocation has not been simulated. Another important consideration is the day-to-day variability of the environmental models; it is undesirable to underdesign a system such that it is near a performance cliff or over-specify the system which will unnecessarily add to its cost. The next section presents analysis which accounts for the first three of the above considerations, the last (environmental variability) is discussed by Francis et al. (2017).

5.2. Radar Tasking and Mission Scenarios

OTH radar are typically tasked to monitor several footprints or tiles in their field of regard and operate in a step scan mode whereby each footprint is revisited in a schedule (typically 30 s; Skolnik, 2008). The size of these tiles will depend upon the operating frequency and the level of ionospheric support. Typically, the range depth is 300–400 km and the azimuth extent 8–10°. The important point to note, however, is that each footprint is monitored, necessarily, by a single frequency and so the SNR of a target will depend upon where it is within the footprint. We account for this effect by tiling the field of regard in an appropriate way suitable for the mission and choose the appropriate model frequency for each tile. As we are now optimizing over a 2-D space, the algorithm is more sophisticated than the simple 1 MHz back from the leading edge discussed in the previous section. The optimal frequency is that which maximizes the modeled SNR across all range-azimuth cells of the tile. OTH radar are generally operated in conjunction with environmental support instruments such as HF ionospheric back scatter sounders, which characterize the propagation conditions. These systems enable the OTH radar operator to select the best frequency for the task (Earl & Ward, 1987).

Figure 12 displays an example of how one may lay down tiles for the New Zealand radar surveilling the Australian eastern seaboard. A total of eight tiles are displayed here which yields a revisit rate of 32 s for a CIT of 4 s. Reducing the CIT will enable more of the field of regard of the radar to be surveilled; however, this is at the

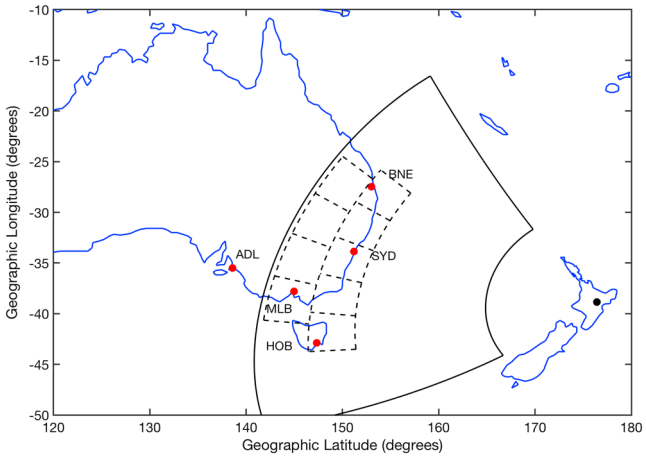

Figure 12. Example of tasking an over-the-horizon radar. The solid black lines indicate the notional coverage (or field of regard) of a typical over-the-horizon radar. The dashed black lines the indicate surveillance footprints (or tiles) that the radar will step scan with a typical revisit interval of ~ 30 s.

expense of SNR and hence the probability of mission success (i.e., tracking the targets) will drop. This drop in SNR can be recovered by increasing the transmit power or the array sizes etc. with an associated increase in cost for the system.

Note that there will be a transmit beam shape loss across the tiles. We do not account for this in the modeling presented here. The half-power full-width of the transmit beam beam will vary as a function of frequency; e.g., a 90-m linear array with a 20-dB taper across the aperture for sidelobe control will have beam widths of ~ 15° and 8° at the extrema of the frequency band of our hypothetical system (13 – 26 MHz).

For targets that are not obscured by ground clutter (i.e., radial speed > 43.6 km/hr) we apply a tracker model to determine if the targets will be successfully tracked. We use a simple M detections out of N observations tracker (e.g., Davey, 2013), where $M = 7$ and $N = 10$ with a mission success criterion of 90%. The noise is assumed to be Gaussian for our tracker model.

For a given season and solar activity level we determine for each radar the probability that the target will be tracked at each point along its flight path at each hour of the day. This allows us to calculate the probability of the target being tracked at a network level, that is, the probability of at least one radar tracking the target. If this exceeds our mission success criterion of 90%, we deem that the target is successfully tracked by the radar network. This allows us to calculate the number of hours per day that the target will be expected to be tracked by the radar network at each point along the target's flight path.

We apply this analysis to the hypothetical OTH radar network defined in section 2. Figure 13 displays the results for Boeing 777 aircraft flying inbound to Sydney from other major Australian cities under various ionospheric conditions. For all cases, the aircraft are flying straight and level at a constant speed of 900 km/hr. We note that this analysis makes no statement as to the utility of each radar in tracking a particular target. However, that sort of analysis is straightforward (discussed in Francis et al., 2017), and if it showed, for instance, that a particular radar has a low probability of tracking the target, then one might consider allocating its resource elsewhere.

We note from inspection of Figure 13 two points: (1) the success rate for tracking the targets is, not surprisingly, higher for better propagation conditions and (2) during times of poor ionospheric support the aspect sensitivity of the target RCS is an important factor as to how often the target will be tracked at each point in its flight path. The first point, while not surprising, is important. If it is a requirement of the system to track the targets during poor propagation conditions (e.g., winter solar minimum), then this analysis can help to design the radar system do so. As discussed previously with respect to Figure 7, it may be necessary to construct a low-band transmit array to allow operations at frequencies down to 5 MHz during the times when the ionosphere does not support propagation at frequencies above the minimum of our single band transmit system.

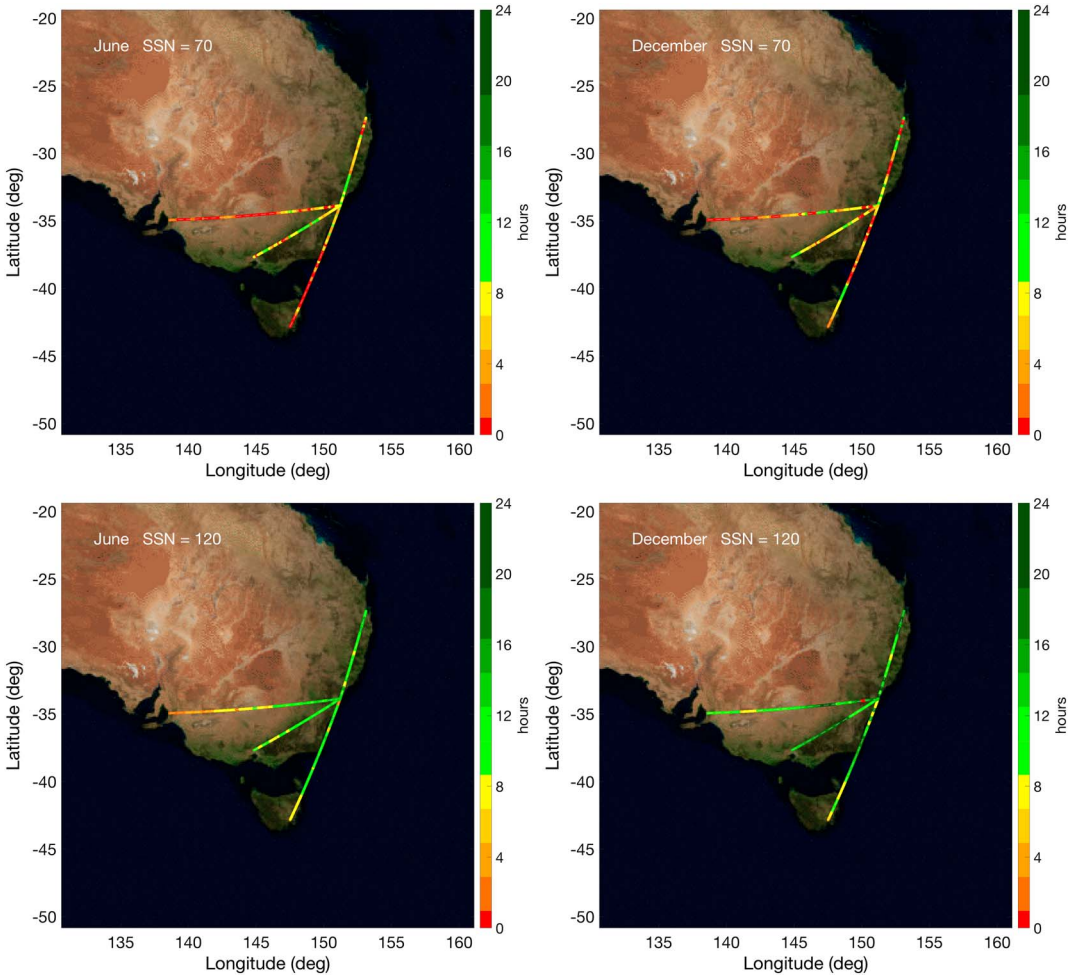

Figure 13. Expected number of hours per day that the hypothetical over-the-horizon radar network will successfully track Boeing 777 aircraft flying inbound to Sydney from other major Australian cities for different propagation conditions. SSN = smoothed sunspot number.

5.3. Discussion

The hypothetical OTH radar network that we have modeled in this paper is clearly marginal for the mission. While it is able to successfully track Boeing 777 aircraft flying routes along the Australian eastern seaboard during solar maximum conditions, it struggles at lower levels of solar activity. Indeed, it completely fails during solar minimum conditions (not shown here). Additionally, many commercial aircraft flying these routes are smaller aircraft (Boeing 737 and similar in size). These aircraft would be even more difficult to track under poor to moderate solar conditions. The reason we chose to model an underspecified system for times of poor ionospheric support was to highlight and draw out the various issues which can potentially impact an OTH radar network.

If one were to consider building such a system it would need to be a scaled up version. One might consider greater transmit power, a second low-band transmit array, a larger receive array with greater directive gain, or a combination of these. Alternatively, notwithstanding the fact that there are limited choices for the siting of the radars in our hypothetical scenario, in general additional sites could improve the overall network performance at times when the propagation conditions are not so poor that there is no propagation support at all, but poor enough that target RCS aspect sensitivity is an issue. The question then is what is the cost-benefit ratio of more smaller systems in the network versus fewer larger systems. The modeling methodology described in this paper would be suitable to assess such a scaled up systems and overall network design.

Another option for system sensitivity improvement is to employ recent advances in the signal processing algorithms, which may recover some of the tapering losses through various autoregressive data extrapolation

techniques. These are (1) complex time series data extrapolation to reduce the Doppler taper loss (Turley, 2008), (2) bandwidth extrapolation to reduce the range taper loss (Nguyen & Turley, 2015), and (3) aperture extrapolation (Nguyen et al., 2016) to reduce the digital beamforming taper loss. It is beyond the scope of this paper to model these techniques.

6. Conclusion

We have described a radio wave propagation-based climatological model for OTH radar systems and have applied it to a hypothetical radar network. The environmental conditions (which impact propagation) were considered and form the basis of the model. However, we showed that for an OTH radar model to give a realistic assessment against a particular surveillance mission, it is important to consider aspect sensitive target RCSs, appropriate allocation of the radar resources, and an appropriate target tracker model. The model forms the first step of a sophisticated radar network design methodology. Other applications of the modelling methodology include the assessment of existing systems and integration of realistic OTH models into wargaming simulation frameworks.

Acknowledgments
The authors wish to acknowledge earlier work by staff of the Defence Science and Technology Group, Australia, and the ROTHR Program Office, United States. We thank C. Williams for the generation of the target model RCS data and antenna patterns. The PHaRLAP ray tracing tools and CMOR model are owned by the Australian Commonwealth Government, Department of Defence. They can be made available on a case-by-case basis by contacting the first author at manuel.cervera@dst.defence.gov.au.

References

Bilitza, D., Altadill, D., Zhang, Y., Mertens, C., Truhlik, V., Richards, P., et al. (2014). The international reference ionosphere 2012—A model of international collaboration. *Journal of Space Weather and Space Climate*, *4*(A07), 1–12.

Burke, G., Poggio, A., Logan, J., & Rockway, J. (1979). NEC - numerical electromagnetics code for antennas and scattering. In *Antennas and propagation society international symposium* (Vol. 7, pp. 147–150). Seattle, WA.

Cervera, M. A., & Harris, T. J. (2014). Modeling ionospheric disturbance features in quasi-vertically incident ionograms using 3-D magnetoionic ray tracing and atmospheric gravity waves. *Journal Geophysical Research: Space Physics*, *119*, 431–440. https://doi.org/10.1002/2013JA019247

Coleman, C. J. (1997). On the simulation of backscatter ionograms. *Journal of Atmospheric and Solar: Terrestrial Physics*, *59*, 2089–2099. https://doi.org/10.1016/S1364-6826(97)00038-2

Coleman, C. J. (1998). A ray tracing formulation and its application to some problems in over-the-horizon radar. *Radio Science*, *33*, 1187–1198. https://doi.org/10.1029/98RS01523

Davey, S. (2013). SNR limits on kalman filter detect-then-track. *IEEE Signal Processing Letters*, *20*(8), 767–770.

Davies, K. (1990). *Ionospheric radio*. London: Peter Peregrinus.

Earl, G. F., & Ward, B. D. (1987). The frequency management system of the Jindalee over-the-horizon backscatter HF radar. *Radio Science*, *22*, 275–291. https://doi.org/10.1029/RS022i002p00275

Fabrizio, G. (2013). *High frequency over the horizon radar: Fundamental principles, signal processing, and practical applications*. New York: McGraw-Hill.

Francis, D. B., Cervera, M. A., & Frazer, G. J. (2017). Performance prediction for design of a network of skywave over-the-horizon radars. *IEEE Aerospace and Electronic Systems*, *32*, 18–28.

George, P. L., & Bradley, P. A. (1974). A new method of predicting the ionospheric absorption of high frequency waves at oblique incidence. *Telecommunication Journal*, *41*, 307–311.

International Telecommunication Union (2013). Recommendation ITU-R P.372-11: Radio noise (Tech. Rep.). Geneva, Switzerland: International Telecommunication Union.

Krauss, J. D. (1998). *Antennas* (2nd ed.). New York: McGraw-Hill.

Lomasney, J. M., & Sweeney Jr, L. E. (1973). The twin-whip endfire receiving pair TWERP (Tech. Rep. IDL-TN-3). Menlo Park, CA: Stanford Research Institute.

Lucas, D. L., Prinson, G. S., Headrick, J. M., & Thomason, J. F. (1993). RADARC HF ionospheric prediction program for OTH radar (*Tech. Rep. NRL/MR/5309–93-7316*). Washington DC.

Nguyen, V. K., & Turley, M. D. E. (2015). Bandwidth extrapolation of LFM signals for narrowband radar systems. *IEEE Transactions on Aerospace Electronic Systems*, *51*, 702–712. https://doi.org/10.1109/TAES.2014.130525

Nguyen, V. K., Turley, M. D. E., & Fabrizio, G. A. (2016). A new data extrapolation approach based on spectral partitioning. *IEEE Signal Processing Letters*, *23*, 454–458. https://doi.org/10.1109/LSP.2016.2533602

Nickisch, L. J., St. John, G., Fridman, S. V., Hausman, M. A., & Coleman, C. J. (2012). HiCIRF: A high-fidelity HF channel simulation. *Radio Science*, *47*, RS0L11. https://doi.org/10.1029/2011RS004928

Pederick, L. H., & Cervera, M. A. (2016). A directional HF noise model: Calibration and validation in the Australian region. *Radio Science*, *51*, 25–39. https://doi.org/10.1002/2015RS005842

Skolnik, M. I. (2008). *Radar handbook* (3 ed). New York: McGraw-Hill.

Turley, M. D. E. (2008). Signal processing techniques for maritime surveillance with skywave radar. In *2008 International Conference on Radar* (pp. 241–246). Adelaide, Australia. https://doi.org/10.1109/RADAR.2008.4653925